Atmos. Chem. Phys. Discuss., https://doi.org/10.5194/acp-2019-155
Manuscript under review for journal Atmos. Chem. Phys.
Discussion started: 4 March 2019
© Author(s) 2019. CC BY 4.0 License.

Atmospheric Chemistry and Physics Discussions

Vertical distribution of atmospheric particulate matters within urban boundary layer in southern China: size-segregated chemical composition and secondary formation through cloud processing and heterogeneous reactions

Shengzhen Zhou[1,8*], Luolin Wu[1], Junchen Guo[1], Weihua Chen[2], Xuemei Wang[2*], Jun Zhao[1], Yafang Cheng[2,7], Zuzhao Huang[3], Jinpu Zhang[4], Yele Sun[5], Pingqing Fu[6], Shiguo Jia[1], Yanning Chen[4], Junxia Kuang[4]

[1] School of Atmospheric Sciences, and Guangdong Province Key Laboratory for Climate Change and Natural Disaster Studies, Sun Yat-sen University, Guangzhou, 510275, P. R. China

[2] Institute for Environmental and Climate Research, Jinan University, Guangzhou, 511443, P. R. China

[3] Guangzhou Environmental Technology Center, Guangzhou, 510180, P. R. China

[4] Guangzhou Environmental Monitoring Center, Guangzhou, 510030, P. R. China

[5] State Key Laboratory of Atmospheric Boundary Layer Physics and Atmospheric Chemistry, Institute of Atmospheric Physics, Chinese Academy of Sciences, Beijing, 100029, P. R. China

[6] Institute of Surface-Earth System Science, Tianjin University, Tianjin, 300072, P. R. China

[7] Multiphase Chemistry Department, Max Planck Institute for Chemistry, P.O. Box 3060, Mainz, 55128, Germany.

[8] Southern Laboratory of Ocean Science and Engineering (Guangdong, Zhuhai), 519082, P. R. China

Correspondence to: Shengzhen Zhou (zhoushzh3@mail.sysu.edu.cn) and Xuemei Wang (eeswxm@mail.sysu.edu.cn)

Abstract. Great progress has been made recently in the understanding of the sources and formation mechanisms of atmospheric aerosols at the ground level. However, vertical profiles and sources of size-resolved particulate matter within the urban boundary layer are still lacking. In this study, vertical distribution characteristics of size-segregated particles were investigated at three observation platforms (ground, 118 m and 488 m) on the 610-meter-high Canton Tower in Guangzhou, China. Size-segregated aerosol samples were simultaneously collected at the three levels on the Canton Tower in autumn and winter, respectively. Major aerosol components, including water-soluble ions, organic carbon and elemental carbon, were measured. The results showed that daily average fine-particle concentrations generally decreased with height. Concentrations of sulfate and ammonium in fine particles displayed

Atmos. Chem. Phys. Discuss., https://doi.org/10.5194/acp-2019-155
Manuscript under review for journal Atmos. Chem. Phys.
Discussion started: 4 March 2019
© Author(s) 2019. CC BY 4.0 License.

Atmospheric Chemistry and Physics Discussions

small vertical gradients and nitrate concentrations increased with height in autumn, while the above chemical components showed greater variations in winter than in autumn. The size distributions of sulfate and ammonium in both seasons were characterized by dominant unimodal droplet modes with a peak at the size range of 0.44–1.0 μm. In autumn, the nitrate size distribution was bi-modal, peaking at 0.44–1.0 μm and 2.5–10 μm, while it was unimodal in winter, implying that the formation mechanisms for nitrate particles were different in the two seasons. Our results suggest droplet mode sulfate and nitrate are likely formed from aqueous-phase reactions and coarse mode nitrate formation is attributed to heterogeneous reactions of gaseous nitric acid on existing sea-derived coarse particles in autumn at the measurement site. The results from pollution cases study further showed that atmospheric aqueous-phase and heterogeneous reactions together with adverse weather conditions, such as temperature inversion and calm wind, resulted in the autumn and winter haze pollution in the PRD region.

1 Introduction

Air pollution is of serious environmental concern in China and it is often characterized by high concentrations of many pollutants, among which fine particulate matter (particles with the aerodynamic diameter of 2.5 μm and smaller or $PM_{2.5}$) is currently the primary pollutant at most of the cities. Aerosol particles can profoundly affect public health, visibility, and climate change, and their effects are strongly dependent on the size distribution and chemical composition of the particles (Pöschl, 2005; Zhang et al, 2015). The particulate matter (PM) chemical constituents include sulfate, nitrate, ammonium, organic matter, elemental carbon, crustal species, and trace metals, which have a variety of primary and secondary sources from either nature or human activities. Although the sources and formation mechanisms of atmospheric particles have been extensively investigated, it remains highly uncertain in the fine size regime (Huang et al., 2014; Liang et al., 2016; Sun et al., 2015; Tian et al., 2016; Zhang et al., 2015).

The size-resolved PM chemical composition is a key factor to understand the sources, formation, and transformation of atmospheric particles (Seinfeld and Pandis, 2006; Cabada et al., 2004; Wang et al., 2014). Typically, the mass distribution of airborne particles is dominated by two modes: the accumulation mode (~0.1 to ~2 μm) and the coarse mode (~2 to ~50 μm) (Seinfeld and Pandis, 2006).

© Author(s) 2019. CC BY 4.0 License.

However, in many cases, the accumulation mode consists of two overlapping sub-modes: the condensation mode and droplet mode. The condensation mode is generally from gas-to-particle conversion or directly emitted from combustion, while the droplet mode is mainly contributed from cloud processing or coagulation of smaller particles. The two sub-modes were firstly reported for sulfate particles (0.2 ± 0.1 μm for condensation mode and 0.7 ± 0.2 μm for droplet mode) (Hering and Friedlander, 1982; John et al., 1990). Moreover, particles measured at many worldwide locations were shown in the droplet mode (Meng and Seinfeld, 1994; Zhuang et al., 1999a; Yao et al., 2003; Guo et al., 2010; Tian et al., 2016). Coarse-mode particles with large and irregular sizes, such as sand and sea salt, are usually produced from mechanical processes; however, coarse-mode secondary sulfates and nitrates were also observed, and their formation was attributed from heterogeneous and multiphase reaction mechanisms (Liu et al., 2008; Pakkanen, 1996).

Measurements of ambient particles at several heights rather than just at a single ground level provide unique information about their sources and dynamic transport. In addition, the vertical PM distribution can reflect the influences of atmospheric boundary meteorology on aerosol chemistry. Vertical profiles of atmospheric pollutants were frequently measured in tall towers located in urban areas. For instance, based on measurements in the 325-m meteorological tower located in urban Beijing, Chan et al. (2005) showed a complex vertical distribution of fine PM and carbonaceous species in it over the city. Sun et al. (2015) conducted real-time and simultaneous vertical measurements of aerosol particles at the ground level and at 260 m on this tower and showed very dynamic vertical profiles of meteorological parameters below 300 m which affected the formation and evolution processes of aerosols during the haze episodes (Wang et al., 2018; Sun et al., 2015). A series of vertical measurement of atmospheric particulate matter and meteorological parameters on a 255 m meteorological tower in the Tianjin have been carried out in recent years (Zhang et al, 2011; Shi et al, 2012; Wang et al, 2016). Oztürk et al (2013) conducted high-resolution measurements of aerosol particle composition using a compact time-of-flight aerosol mass spectrometer and found considerable variability in the vertical distribution of aerosol mass concentration and composition on a 265-m tall tower near suburban Denver, Colorado. Deng et al. (2014) reported the vertical distribution of PM_{10}, $PM_{2.5}$ and $PM_{1.0}$ mass concentrations measured on Canton Tower at 121 and 454 m from November

© Author(s) 2019. CC BY 4.0 License.

2010 to May 2013. However, measurements of the vertical size-resolved chemical composition within the urban boundary layer are still lacking. Wang et al. (2016) investigated the size distribution of chemical compositions and sources of particulate matters in different mode at the ground level and 220 m in Tianjin. They suggested that the 220 m height is not high enough to eliminate the influence of local surface emissions and reflect the background levels of pollutants within urban canopy.

The Pearl River Delta (PRD) region is the low-lying area surrounding the Pearl River estuary, where the Pearl River flows into the South China Sea. The weather here is generally warm and humid all year and is strongly influenced by the Asian monsoon. The PRD region is one of the most densely urbanized regions in the world, which has recently been experiencing severe PM pollution and photochemical smog events (Zhang et al., 2008; Huang et al., 2014; Zhou et al, 2014). Autumn and winter are typical pollution seasons in this region (Chan et al, 2008). In this study, size-resolved PM samples were collected at three heights (the ground level, 118 m, and 488 m) on Canton Tower in Guangzhou, the central city in the PRD region. The main water-soluble ions (Na^+, K^+, Mg^{2+}, Ca^{2+}, NH_4^+, F^-, Cl^-, NO_2^-, NO_3^-, SO_4^{2-}) and carbonaceous species (organic carbon, OC; elemental carbon, EC) were measured and their chemical characteristics, formation mechanisms and sources were shown. The objectives of this work were (1) to study the vertical mass size distribution of the PM chemical components and (2) to investigate the factors on the vertical variations of PM and their implications to the local haze formation. Our study is unique in the measurement of size-resolved PM components at the height of nearly 500 m above ground level, where they can be strongly influenced by the dynamic variations of atmospheric boundary layer and cloud processing.

2 Methodology

2.1 Observational site and sample collection

The sampling site, Canton Tower, is located in central urban Guangzhou and is the second highest TV tower in the world with a total height of 610 m. The main tower is 454 m high and the antenna mast adds another 156 m. Four levels (the ground level, the other three levels at 118 m, 168 m, and 488 m) were selected by the Guangzhou Environmental Protection Bureau to set up vertical gradient observation platforms at respective heights. Online measurements of pollutants including SO_2 (model

© Author(s) 2019. CC BY 4.0 License.

43i, Thermo), CO (model 48i, Thermo), O_3 (model 49i, Thermo), NO/NO_x (model 42i, Thermo), PM ($PM_{2.5}$ and $PM_{1.0}$, SHARP 5030, Thermo) were conducted on this four-layer observation platform. Meteorological factors (relative humidity, temperature, wind speed and direction) were also recorded on the tower. All these data were applied for the discussions in the following sections.

In this study, size-segregated aerosol samples were concurrently collected at the ground level, 118 m and 488 m in autumn (October and November 2015) and winter (December 2015 and January 2016) seasons (Fig. 1). Three six-stage samplers (Model 131 High-Flow Impactor, MSP Corporation) with a sampling flow rate of 100 L min^{-1} were used at the three heights. The samplers were calibrated and compared before the usage. The 50% cut-point diameters of the six-stage sampler are 0.25, 0.44, 1.0, 1.4, 2.5, 10.0 and 18.0 (inlet) μm. A 24-h sampling resolution was adopted every other day from 10:00 a.m. to 10:00 a.m. of the next day (local time, UTC + 8). The collection substrates were 75-mm diameter quartz filters and a final 90-mm quartz filter was applied to collect aerosols with diameters of less than 0.25 μm. All the quartz membrane filters were prebaked at 550 ℃ for 4 hours before use to eliminate possible organic contaminants. In total, 19 and 13 sets of samples including one set of background samples were collected at each height in autumn and winter, respectively. After collection, the filters were put into Petri dishes, kept in ice boxes during transportation to the laboratory and then stored in a refrigerator at -18 ℃ prior to analysis.

2.2 Chemical analysis

A quarter of each quartz filter was cut out and dissolved in 15 mL deionized water (18.2 MΩ, Millipore) for 30 min in an ultrasonic ice water bath. The extracted solution was filtered through a microporous membrane (pore size, 0.2 μm) into a clean polycarbonate bottle, and then analyzed by an ion-chromatograph (ICS-5000, Dionex). The cations (Na^+, K^+, Ca^{2+}, Mg^{2+}, NH_4^+) were separated using a CS12A column (4 × 250 mm) and eluted with KOH solution. The anions (F^-, Cl^-, NO_3^-, NO_2^- and SO_4^{2-}) were analyzed using an AS23 column (4 × 250 mm) and eluted with a methane sulfonic acid solution. Multiple points of calibration were used for each batch of ionic analysis. The OC and EC mass concentrations were determined using a thermal optical carbon analyzer (DRI Model 2001A, Atmospheric Inc., USA). The analysis procedures were described in detail in Chow et al. (2001) and Cao et al. (2004). Due to the non-uniform deposition nature of the size resolved samplers, charring

© Author(s) 2019. CC BY 4.0 License.

correction using optical transmittance may introduce uncertainty for determining the OC and EC split point (Huang et al, 2009). The data presented in this paper were all field-blank corrected.

2.3 Data analysis

Back-trajectory analysis was performed using the Hybrid Single-Particle Lagrangian Integrated Trajectory model (HYSPLIT 4.9) (Draxler and Hess, 1998). The Global Data Assimilation System (GDAS, $1^o \times 1^o$) was used for the input meteorological data and 72-h air mass back-trajectories were calculated at starting times of 02:00, 08:00, 14:00 and 20:00 (UTC), with arrival heights of 200 and 500 m above ground level. A cluster analysis was performed to segregate the calculated trajectories into distinct cluster groups using the HYSPLIT clustering algorithm.

To study the effects of meteorology, vertical profiles of wind direction and speed, relative humidity (RH) and temperature (T) were simulated by the Weather Research and Forecasting (WRF) Model (Skamarock et al, 2008). The detailed information about the model setup can be found in the supplementary materials and references (Fan et al, 2015; Chen et al, 2016).

3 Results and discussion

3.1 General characteristics

Figure 2 shows the temporal profiles of daily averaged $PM_{2.5}$ mass concentrations measured at the three heights during the sampling periods. A polluted episode (i.e., E1) in autumn was identified as the $PM_{2.5}$ concentration at the ground level exceeded the air quality standard (75 μg m^{-3}), while another episode (i.e., E2) occurred during continuous three exceeding-standard days in winter. The average $PM_{2.5}$ mass concentrations were 42.4, 34.5 and 26.5 μg m^{-3} at the ground level, 118 m and 488 m respectively in autumn, slightly higher than those in winter (42.1, 33.7 and 22.5 μg m^{-3} at the respective levels). Overall, the average $PM_{2.5}$ concentrations decreased with height, consistent with previous studies (Deng et al., 2014; Chan et al., 2005; Wang et al., 2016). The diurnal variations of $PM_{2.5}$ and $PM_{1.0}$ concentrations at the three heights in autumn and winter are shown in Figs. S1 and S2. In general, $PM_{2.5}$ and $PM_{1.0}$ concentrations at the ground level and 118 m showed distinct diurnal cycles with higher concentrations occurred at rush hours in the morning and evening. However, the ones at 488 m

© Author(s) 2019. CC BY 4.0 License.

showed unimodal distribution with higher concentrations observed in the afternoon (12:00-17:00), 3-4 hours lagging behind those at the ground level and 118 m. This can be attributed to the facts that the convective boundary layer begins to extend vertically after sunrise, and particles were transported upward by turbulence. The diurnal variations of CO and NO_x showed similar trends with the PMs. The O_3 diurnal cycle showed a single peak pattern at the three levels with the highest values at around 14:00 LST. The O_3 concentrations were higher at 488 m than at the lower levels. The O_3 concentration gaps between the lower levels and 448 m were widened at night due to the intensive NO titration loss at lower levels (Figs. S1 and S2).

3.2 Vertical distribution

3.2.1 Vertical distribution of the major chemical compositions

Figure 3 shows the representative and average vertical profiles of $PM_{2.5}$, sulfate, ammonium, nitrate, OC, and EC mass concentration on the tower. Shallow vertical gradients for sulfate and ammonium were observed in autumn (Fig. 3a). Higher concentrations for nitrate in both fine and coarse modes were found at higher levels. A typical case was on November 18, 2015, when the air quality did not meet the air quality standard. Nitrate concentration was 1.5 times higher at 488 m than at ground level. In particular, the nitrate concentration was 1.5 times higher at 488 m than that at ground level for the polluted episode E1 on November 18, 2015, which will be discussed in detailed later. Much steeper vertical gradients were found for OC and EC compared to sulfate and ammonium, with the EC concentration 27.9% lower at 488 m than at ground level and OC concentration 34.0% lower at 488 m than at ground level. The decrease in air pollutant concentrations with height is considered to be associated with ground-level sources, such as EC from diesel exhaust (Zauli Sajani et al., 2018).

The $PM_{2.5}$ chemical components showed more complex vertical gradients in winter than in autumn (Fig. 3b). The vertical gradients can be classified into four categories based on the component profiles. For the first one, the $PM_{2.5}$ components decreased with height, such as SNA on January 25, 2016 (not shown); for the second one, the PM components increased with height, such as SNA on December 31, 2015. The third one, however, an increase in concentration at the middle 118 m level and then a decrease at 488 m were observed, i.e., the profiles on January 2, 2016. No obvious vertical gradients for all measured PM components during clean days were found (e.g., those on October 31, 2015 and

© Author(s) 2019. CC BY 4.0 License.

January 17, 2016). The homogenous distribution of aerosol composition is resulted from the turbulent mixing of air pollutants within the boundary layer (Guinot et al., 2006).

3.2.2 Chemical composition in fine and coarse aerosols

Figure 4 shows the percentages of measured chemical composition in fine ($PM_{2.5}$) and coarse ($PM_{2.5-18}$) particles at the three heights (the ground level, 118 m, and 488 m). OC, sulfate and EC were the major chemical components of fine particles in autumn. Elevated proportions of nitrate and ammonium were found in winter, possibly related to the equilibrium between gas phase HNO_3 and NH_3 and the particle phase. During our sampling periods, the average temperature in winter (13.5 ℃) was much lower than that in autumn (23.1 ℃), resulting in the enhanced production of NH_4NO_3 particles (Bian et al, 2014). The relative contributions of the main chemical components of fine particles at the ground level and 118 m did not show significant differences. We found that the total contribution of SO_4^{2-}, NO_3^- and NH_4^+ at 488 m were higher than those at the two lower levels, indicating the favorable secondary formation or regional transport of aerosols at the higher altitude. Our results showed that OC, nitrate, crustal (e.g., Ca^{2+}, Mg^{2+}), sea salt (e.g., Na^+ and Cl^-) were the major components of coarse particles. The percentages for nitrate and sea salts were higher in autumn than those in winter, suggesting that sea salt would be a nonnegligible source for aerosols in autumn in the PRD region. We also found that the fractions of primary inorganic ions (e.g., Ca^{2+}) and EC in coarse particles decreased with height, due probably to their sources (e.g., road dust and traffic emissions) near the ground.

3.2.3 Mass size distributions

Aerosol chemical components from different sources and with different formation mechanisms may lead to different mass size distributions. The average mass size distribution of the ionic compounds, OC and EC at the three heights during the autumn and winter field studies are shown in Figs. 5 and 6.

(1) Sulfate, nitrate, and ammonium

Sulfate did not show obvious seasonal and vertical variations in mass size distribution (Figs. 5 and 6). The average mass size distributions of SO_4^{2-} were shown to be a dominant peak in the range of 0.44–1.0 μm (a typical droplet mode) and a minor coarse mode in the range of 2.5–10 μm. The mass size distributions of sulfate at the three levels were similar, indicating that sulfate may have similar

© Author(s) 2019. CC BY 4.0 License.

formation mechanisms. Previous studies showed that droplet-mode sulfate could be formed in cloud or fog (Zhuang et al., 1999a; Kerminen and Wexler, 1995; Meng and Seinfeld, 1994). Guo et al (2010) proposed three possible formation processes for droplet-mode sulfate, including condensation and coagulation of smaller particles, in-cloud aqueous processes and processes in deliquesced aerosol particles. Using the positive matrix factorization (PMF) method similar to the one described in Guo et al (2010), we obtained three modes (i.e., condensation, droplet, and coarse modes) for the sulfate size distribution, among which the droplet mode accounted for 79.4%, 78.5%, 86.9% in autumn, and 78.5%, 78.3%, 80.4% in winter respectively at the ground level, 118 m and 488 m (Table 1S). Besides, high relative humidity (~78% and 80% in average) was measured respectively during the autumn and winter measurement periods in Guangzhou. The contribution of droplet mode sulfate was higher at 488 m than that at two lower levels, leading to the conclusion that in-cloud or aerosol droplet processes is likely the main formation pathways for sulfate with evidences of frequent cloud coverages at 500-1000 m above the ground in urban Guangzhou measured using a ceilometer during the measurement periods (Tao et al., 2018).

The mass size distribution for nitrate exhibited two modes with mass median aerodynamic diameters at 0.44–1.0 μm (fine mode) and 2.5–10 μm (coarse mode) in autumn, while fine mode pattern peaking at around 1.0 μm was observed in winter. The coarse-mode nitrate in autumn accounted for ~ 63%, 58%, and 58% of the total nitrate measured at the ground level, 118 m and 488 m, respectively. It has been proposed that coarse-mode nitrate was formed through the reactions of gaseous nitric acid on pre-existing sea- and soil-derived coarse particles (Anlauf et al., 2006; Pakkanen, 1996; Zhuang et al., 1999a). NaCl particles usually represent sea salt. As shown below is reaction between nitric acid and sea salt particles (Wall et al., 1988; Pakkanen, 1996; Harrison and Pio, 1983):

$$HNO_3(g) + NaCl(s) \rightarrow NaNO_3(s) + HCl(g) \quad (1)$$

Other studies suggested that gaseous nitric acid may react with soil-derived coarse particles via the following reaction (Wu and Okada, 1994; Harrison and Kitto, 1990; Pakkanen, 1996):

$$HNO_3(g) + CaCO_3(s) \rightarrow Ca(NO_3)_2(s) + H_2O(aq) + CO_2(g) \quad (2)$$

We found that coarse-mode Na^+, Cl^- and NO_3^- were measured at almost the same particle size, while Ca^{2+} peaked at a particle size larger than NO_3^- in this study (Fig. S3). It is hence reasonable to conclude

© Author(s) 2019. CC BY 4.0 License.

that coarse-mode NO_3^- is probably associated with sea salt rather than Ca^{2+}, which was also consistent with the previous work in Hong Kong (Zhuang et al., 1999b). The back-trajectory cluster analysis showed that the sampled air masses were predominantly from the South China Sea towards Guangzhou in autumn (Fig. S4), which brought high concentrations of sea salt particles for heterogeneous reactions. In addition, sea-salt particles can be activated to cloud or fog droplets under certain supersaturation conditions (Zhuang et al., 1999b). Hence, nitrates were probably formed from the reactive uptake of HNO_3 in the deliquesced sea salt droplets rather than dry particles in Guangzhou, as previous study showed formation of substantial amount of nitrates when HNO_3 reacted with the deliquesced sea-salt compared to the dry NaCl particles (Brink, 1998). Besides, other factors such as high relative humidity, fog, and low clouds could facilitate the formation of deliquesced sea salt particles which then accelerate the heterogeneous formation of coarse mode nitrates.

In winter, the mass size distribution for nitrate was dominated by the droplet mode (the size range of 0.44–1.0 μm), contrast to a relative small nitrate peak in this mode in autumn (Figs. 5 and 6). Previous studies showed that droplet mode nitrate could be produced by condensation of nitric acid onto pre-existing particles and/or heterogeneous reactions of N_2O_5 (Guo et al, 2010, Wang et al, 2012). Yun et al (2018) pointed out the important contribution of heterogeneous uptake of N_2O_5 to nitrate formation during the winter haze in the PRD region. Based on the mass size distribution for nitrate and high relative humidity, we speculated that hydrolysis of N_2O_5 would also be an important mechanism for nitrate formation in the PRD region in winter. The contribution of heterogeneous reactions between nitric acid and sea salt droplets was minor in winter based on the factor that the air masses were predominantly from inland (Fig. S4), bringing a much lower concentration of coarse mode sea salt aerosols than that in autumn (Figs. 5 and 6). Therefore, the heterogeneous reactions of nitric acid with sea salt droplets were less important in winter. Although fine mode NH_4^+ ions were found to be dominant in the mass size distribution in both autumn and winter, the concentration of fine mode NH_4^+ ions was strongly correlated with that of the same mode SO_4^{2-} ($R > 0.89$ at three heights), while only moderately correlated with that of fine mode NO_3^- ions in autumn, implying that fine mode nitrates exist not only as NH_4NO_3 but also as other forms (i.e., $NaNO_3$) in autumn.

(2) Sodium and chloride

© Author(s) 2019. CC BY 4.0 License.

The mass size distributions for Na^+ and Cl^- showed distinctly different patterns in autumn and in winter. Na^+ and Cl^- exhibited unimodal peaking in the range of 2.5–10 μm in autumn. The proportion of Na^+ in coarse mode was 63%, 71% and 68% of the total Na^+ mass, and 59%, 69% and 70% of Cl^- ions were observed in coarse mode at the ground level, 118 m and 488 m respectively, indicating that their contributions at the upper levels were higher than those at the ground level. The coarse chloride particles were considered to originate from marine sources and be associated with sodium (Zhao and Gao, 2008; Bian et al., 2014). As discussed above (Fig. S4), ambient air in Guangzhou was strongly influenced by particles from marine sources which were transported from South China Sea in autumn. We calculated the chloride depletion based on the concentrations of Na^+ and Cl^- (Eq. 3) to estimate the nitrate and sulfate formation rates on the sea-salt particles (Zhuang et al, 1999b):

$$[Cl_{dep}] = (1.174[Na^+] - [Cl^-])/1.174[Na^+] \times 100\% \quad (3)$$

where $[Na^+]$ is the measured concentration and 1.174 is the molar ratio of Cl^- to Na^+ in seawater. More chloride depletion (in percentage) was found for larger size of particles (> 1.0 μm) at the highest level (488m) (Fig. S5), suggesting more intensive reactions involving Cl^- ions occurred at this level than other lower levels. In comparison, possible sources for fine-mode chloride particles were from biomass burning, coal combustion and waste incineration (Fu et al., 2018; Zhao and Gao, 2008). The origin of fine chloride particles in winter during the measurement periods however, is complicated based on the broad peaks for Na^+ and Cl^-.

(3) OC and EC

In general, the mass size distributions for OC were found to be unimodal with a peak at 0.44–1.0 μm in which a percentage of 84% and 88% of the total mass was attributed respectively to fine mode in autumn and winter (Figs. 5 and 6). In addition, they showed similarity at the three heights, implying that they probably shared the same origins. Similarly, EC was also mainly in fine mode except that it had a much broader size distribution than that of the OC. Interestingly, there was a sharp peak in the size range of 1.0–1.44 μm in the mass size distribution of the EC at 118 m, suggesting that its source at this level might be different from other levels as we found that the SO_2 and CO concentrations were highest among the three heights (Fig. S6). One possible reason for the abnormal high concentrations for those

© Author(s) 2019. CC BY 4.0 License.

species was the influences from the local point sources (i.e., high chimneys from power plants and factory chimneys) around Guangzhou which emitted elevated concentrations of air pollutants.

3.3 Case studies of PM vertical profile during pollution episodes

Factors that influence vertical distribution of PM include meteorology, regional transport, source emission, and chemical reactions. Here we selected two PM pollution episodes (E1 and E2) to investigate the haze formation in autumn and in winter respectively (Fig. 2). The E1 episode which occurred on November 18, 2015 represented a typical pollution scenario in autumn. An anomaly increase was observed for $PM_{2.5}$ concentration at 168 m compared to the concentrations on non-event days. In addition, the average sulfate, nitrate, and ammonium (SNA) concentrations were higher at 488 m and 118 m than those at the ground level (Fig. 3a). We employed the WRF model to simulated horizontal and vertical wind, RH, and T. The results showed that horizontal southerly wind was prevalent prior to November 18 with a period of calm wind from around 2:00 LST to 14:00 LST and subsequently the wind direction changed predominantly to north after that (Fig. S7), consistent with back trajectory analysis which showed that air masses firstly came from the south and then changed to north at November 19 (Fig. S8). Low altitude temperature inversion was observed between 118 m and 168 m at night probably due to the convergence of two different air streams (Fig. S7). A previous study (Wu et al, 2015) demonstrated that poor air quality was associated with surface and low-altitude inversions in the PRD region. The RH vertical profile decreased from ground to 168 m and became relatively stable between 168 m and 488 m. Subsequently the RH increased until it reached maximum at around 900 m, followed by a sharp decrease (Fig. 7a). We also found a large amount of low cloud cover in November 17 and 18, especially during nighttime (Fig. 8a). The vertical wind blew dominantly upward during nighttime and downward during daytime (Fig. 8a), which facilitated transport of residual particles produced from cloud evaporation to lower altitudes after sunrise. The average sulfur oxidation ratio ($SOR = n\text{-}SO_4^{2-} / (n\text{-}SO_4^{2-} + n\text{-}SO_2)$) during E1 was 0.22, 0.18, 0.12 at the ground level, 118 m, and 488 m respectively, higher than that on non-event days. We noticed that SO_2 concentration increased with height (12.4 μg m^{-3} at ground, 16.1 μg m^{-3} at 118 m and 27.0 μg m^{-3} at 488 m), suggesting there were other SO_2 sources besides surface emissions. The corresponding values for nitrogen oxidation

© Author(s) 2019. CC BY 4.0 License.

ration (NOR = n-NO_3^- / (n-NO_3^- + n-NO_2) was 0.01, 0.02 and 0.07 at the three levels respectively. A number of previous studies demonstrated that high relative humidity was in favour of the production of secondary aerosols (Sun et al, 2013; Cheng et al, 2016; Zheng et al, 2016). Our results showed that aqueous phase and heterogeneous reactions also significantly contributed to sulfate and nitrate aerosol formation in the PRD region.

The E2 episode represented a typical pollution event in winter, showing a similar $PM_{2.5}$ vertical distribution as E1. Moreover, the highest sulfate, nitrate, ammonium, and OC concentrations were observed at 118 m (Fig. 3b). Horizontal wind was mainly from north before noon (January 2) and changed to south in the afternoon (Fig. S7). In addition, similar temperature and RH profiles were found for the E2 to those for E1 which characterized by low altitude temperature inversion with the thickness from ~168 m to 488 m at Jan 2 and ~ 50 m to 168 m at Jan 3, as well as a higher RH at higher levels during nighttime (Fig. 7b). High amount of low cloud cover and strong convection mixing process were observed during this episode (Fig. 8b). The average SOR in $PM_{2.5}$ was 0.36, 0.27, and 0.30 at the ground level, 118 m and 488 m respectively, again higher than non-event days. The average NOR was 0.13, 0.14, and 0.21 at the ground level, 118 m and 488 m respectively, two or triple times higher than that on non-event days. Based on the above findings, a schematic graph was summarized for illustrating a typical haze formation mechanism in the PRD region in autumn and winter seasons (Fig. 9). Our results suggested that adverse meteorology (such as nighttime temperature inversion and calm wind) together with aqueous phase (cloud processing) and heterogeneous reactions would significantly contribute to the aerosol formation and haze episodes in the PRD region during the measurement periods. However, more studies, such as long-term field measurements and atmospheric chemical model simulations, are warranted on the extent of the impacts of aqueous and heterogeneous reactions on regional air quality and on the radiation budget of the atmosphere in southern China.

4 Conclusions

Utilizing the 610 m Canton Tower in Guangzhou, the vertical characteristics and sources of size-resolved aerosols were studied during autumn and winter seasons. Complex vertical variations in PM composition were observed. Sulfate and ammonium in autumn presented small vertical gradients than

© Author(s) 2019. CC BY 4.0 License.

nitrate, which showed higher concentrations at higher levels. OC and EC showed steeper vertical gradients, with concentrations 34.0% and 27.9% lower, respectively, at 488 m than at the ground level. The chemical composition of the fine particles showed more pronounced and complex vertical gradients in winter than in autumn, possibly due to the effects of atmospheric stability, regional transport, and chemical reactions. The percentages of secondary inorganic ions in fine particles generally increased with height. In contrast, the fractions of Cl^-, Na^+, Ca^{2+} and EC in coarse particles showed a decreasing trend with height. The size distributions of sulfate and ammonium were similar at the three heights during the observation, characterized by a dominant droplet mode. Nitrate showed bi-modal size distributions in autumn and a unimodal pattern in winter, suggesting different nitrate formation mechanisms. Na^+ and Cl^- exhibited dominant unimodal distributions in the range of 2.5–10 μm in autumn, associated with regional transport of sea salt. Na^+ and Cl^- size distributions were dominant in the fine mode in winter. OC and EC were generally in the fine mode with a comparatively broad size distribution. Our study indicated that vertical meteorological parameters, such as RH and T, and the aqueous and heterogeneous atmospheric chemical reactions altogether led to the aerosol formation and haze episodes in the PRD region. The results of this study can help improve understanding the formation of atmospheric aerosols in polluted sub-tropical environments, and can be used to constrain the global models on simulating the aerosol properties.

Author contributions.

SZ and XW designed and led the study. SZ, HZ, JPZ, YC, and JK contributed to aerosols measurement. SZ, JG, and WC carried out the data analysis. LW and WC performed the model simulations. JZ, YFC, YS, PF, and SJ discussed the results and commented on the manuscript. SZ wrote the paper with contributions from all co-authors.

Competing interests.

The authors declare that they have no conflict of interest.

Acknowledgments.

© Author(s) 2019. CC BY 4.0 License.

This work was funded by the National Key Research and Development Program of China (2017YFC0210104, 2016YFC0203305), the National Natural Science Foundation of China (41505106, 21577177), the National Science Fund for Distinguished Young Scholars (41425020), the Fundamental Research Funds for the Central Universities (16lgpy28), and the National Natural Science Foundation as a key project (91644215, 41630422). The authors thank Miss Li Yang and Guo Xu for their support in aerosol samples collection and analysis. We also acknowledge the financial support from Guangzhou Environmental Protection Bureau, the State Key Laboratory of Atmospheric Boundary Layer Physics and Atmospheric Chemistry at Institute of Atmospheric Physics.

References

Andersson, A., Deng, J. J., Du, K., Zheng, M., Yan, C. Q., Sköld, M., and Gustafsson, Ö.: Regionally-Varying Combustion Sources of the January 2013 Severe Haze Events over Eastern China, Environ. Sci. Technol., 49, 2038-2043, doi: 10.1021/es503855e, 2015.

Anlauf, K., Li, S. M., Leaitch, R., Brook, J., Hayden, K., Toom-Sauntry, D., and Wiebe, A.: Ionic composition and size characteristics of particles in the Lower Fraser Valley: Pacific 2001 field study, Atmos. Environ., 40, 2662-2675, https://doi.org/10.1016/j.atmosenv.2005.12.027, 2015.

Bian, Q., Huang, X. H. H., and Yu, J. Z: One-year observations of size distribution characteristics of major aerosol constituents at a coastal receptor site in Hong Kong - Part 1: Inorganic ions and oxalate, Atmos. Chem. Phys., 14, 9013-9027, https://doi.org/10.5194/acp-14-9013-2014, 2014.

Cabada, J. C., Rees, S., Takahama, S., Khlystov, A., Pandis, S. N., Davidson, C. I., and Robinson, A. L.: Mass size distributions and size resolved chemical composition of fine particulate matter at the Pittsburgh supersite, Atmos. Environ., 38, 3127-3141, http://dx.doi.org/10.1016/j.atmosenv.2004.03.004, 2004.

Cao, J. J., Lee, S. C., Ho, K. F., Zou, S. C., Fung, K., Li, Y., Watson, J. G., and Chow, J. C.: Spatial and seasonal variations of atmospheric organic carbon and elemental carbon in Pearl River Delta Region, China, Atmos. Environ., 38, 4447-4456, https://doi.org/10.1016/j.atmosenv.2004.05.016, 2004.

Chan, C. Y., Xu, X. D., Li, Y. S., Wong, K. H., Ding, G. A., Chan, L. Y., and Cheng, X. H.: Characteristics of vertical profiles and sources of $PM_{2.5}$, PM_{10} and carbonaceous species in Beijing, Atmos. Environ., 39, 5113-5124, https://doi.org/10.1016/j.atmosenv.2005.05.009, 2005.

Chan, C. K., and Yao, X. H.: Air pollution in mega cities in China, Atmos. Environ., 42, 1–42, https://doi.org/10.1016/j.atmosenv.2007.09.003, 2008.

Chen, W. H., Wang, X. M., Cohen, J. B., Zhou, S. Z., Zhang, Z. S., Chang, M., and Chan, C.Y.: Properties of aerosols and

© Author(s) 2019. CC BY 4.0 License.

formation mechanisms over southern China during the monsoon season, Atmos. Chem. Phys., 16, 13271–13289, https://doi.org/10.5194/acp-16-13271-2016, 2016.

Cheng, Y. F., Zheng, G. J., Wei, C., Mu, Q., Zheng, B., Wang, Z. B., Gao, M., Zhang, Q., He, K. B., Carmichael, G., Pöschl, U., and Su, H.: Reactive nitrogen chemistry in aerosol water as a source of sulfate during haze events in China, Sci. Adv., 2, e1601530, doi: 10.1126/sciadv.1601530, 2016.

Chow, J. C., Watson, J. G., Crow, D., Lowenthal, D. H., and Merrifield, T.: Comparison of IMPROVE and NIOSH carbon measurements, Aerosol. Sci. Technol., 34, 23-34, http://dx.doi.org/10.1080/02786820119073, 2001.

Deng, X. J., Li, F., Li, Y. H., Li, J. Y., Huang, H. Z., and Liu, X. T.: Vertical distribution characteristics of PM in the surface layer of Guangzhou, Particuology, 20, 3-9, https://doi.org/10.1016/j.partic.2014.02.009, 2014.

Draxler, R. R., and Hess, G. D.: An overview of the HYSPLIT_4 modelling system for trajectories, dispersion, and deposition, Aust. Met. Mag., 47, 295-308, 1998.

Fan, Q., Lan, J., Liu, Y. M. Wang, X. M., Chan, P. W., Hong, Y. Y., Feng, Y. R., Liu, Y. X., Zeng, Y. J., and Liang, G. X.: Process analysis of regional aerosol pollution during spring in the Pearl River Delta region, China, Atmos. Environ., 122, 829-838, https://doi.org/10.1016/j.atmosenv.2015.09.013, 2015.

Fu, X., Wang, T., Wang, S. X., Zhang, L., Cai, S., Xing, J., and Hao, J. M.: Anthropogenic emissions of hydrogen chloride and fine particulate chloride in China, Environ. Sci. Technol., 52, 1644-1654, doi: 10.1021/acs.est.7b05030, 2018.

Guinot, B., Roger, J. C., Cachier, H., Pucai, W., Bai, J. H., and Tong, Y.: Impact of vertical atmospheric structure on Beijing aerosol distribution, Atmos. Environ., 40, 5167-5180, http://dx.doi.org/10.1016/j.atmosenv.2006.03.051, 2006.

Guo, S., Hu, M., Wang, Z. J., Slanina, J., and Zhao, Y. L.: Size-resolved aerosol water-soluble ionic compositions in the summer of Beijing: implication of regional secondary formation, Atmos. Chem. Phys., 10, 947-959, https://doi.org/10.5194/acp-10-947-2010, 2010.

Harrison, R. M., and Pio, C. A.: Size-differentiated composition of inorganic atmospheric aerosols of both marine and polluted continental origin, Atmos. Environ. (1967), 17, 1733-1738, https://doi.org/10.1016/0004-6981(83)90180-4, 1983.

Harrison, R. M., and Kitto, A. M.: Field intercomparison of filter pack and denuder sampling methods for reactive gaseous and particulate pollutants, Atmos. Environ. Part A. General Topics, 24, 2633-2640, https://doi.org/10.1016/0960-1686(90)90142-A, 1990.

Hering, S. V., and Friedlander, S.: Origins of aerosol sulfur size distributions in the Los Angeles basin, Atmos. Environ. (1967), 16, 2647-2656, https://doi.org/10.1016/0004-6981(82)90346-8, 1982.

Huang, R. J., Zhang, Y. L., Bozzetti, C., Ho, K. F., Cao, J. J., Han, Y., Daellenbach, K. R., Slowik, J. G., Platt, S. M., Canonaco, F., Zotter, P., Wolf, R., Pieber, S. M., Bruns, E. A., Crippa, M., Ciarelli, G., Piazzalunga, A., Schwikowski, M., Abbaszade, G., Schnelle-Kreis, J., Zimmermann, R., An, Z. S., Szidat, S., Baltensperger, U., Haddad, I. E., and Prevot, A. S. H.: High secondary aerosol contribution to particulate pollution during haze events in China, Nature, 514, 218-222, doi:10.1038/nature13774, 2014.

© Author(s) 2019. CC BY 4.0 License.

Huang, X. F., and Yu, J. Z.: Size distributions of elemental carbon in the atmosphere of a coastal urban area in South China: characteristics, evolution processes, and implications for the mixing state, Atmos. Chem. Phys., 8, 5843-5853, https://doi.org/10.5194/acp-8-5843-2008, 2008.

John, W., Wall, S. M., Ondo, J. L., and Winklmayr, W.: Modes in the size distributions of atmospheric inorganic aerosol, Atmos. Environ. Part A. General Topics, 24(9), 2349-2359, https://doi.org/10.1016/0960-1686(90)90327-J, 1990.

Kerminen, V. M., and Wexler, A. S.: Growth laws for atmospheric aerosol particles: An examination of the bimodality of the accumulation mode, Atmos. Environ., 29, 3263-3275, https://doi.org/10.1016/1352-2310(95)00249-X, 1995.

Liang, C. S., Duan, F. K., He, K. B., and Ma, Y. L.: Review on recent progress in observations, source identifications and countermeasures of $PM_{2.5}$, Environ. Int., 86, 150-170, http://dx.doi.org/10.1016/j.envint.2015.10.016, 2016.

Liu, S., Hu, M., Slanina, S., He, L. Y., Niu, Y. W., Bruegemann, E., Gnauk, T., and Herrmann, H.: Size distribution and source analysis of ionic compositions of aerosols in polluted periods at Xinken in Pearl River Delta (PRD) of China, Atmos. Environ., 42, 6284-6295, http://dx.doi.org/10.1016/j.atmosenv.2007.12.035, 2008.

Meng, Z. Y., and Seinfeld, J. H.: On the source of the submicrometer droplet mode of urban and regional aerosols, Aerosol. Sci. Technol., 20, 253-265, http://dx.doi.org/10.1080/02786829408959681, 1994.

Öztürk, F., Bahreini, R., Wagner, N. L., Dubé, W. P., Young, C. J., Brown, S. S., Brock, C. A., Ulbrich, I. M., Jimenez, J. L., Cooper, O. R., and Middlebrook, A. M.: Vertically resolved chemical characteristics and sources of submicron aerosols measured on a Tall Tower in a suburban area near Denver, Colorado in winter, J. Geophys. Res.-Atmos., 118, 2013JD019923, doi: 10.1002/2013JD019923, 2013.

Pakkanen, T. A.: Study of formation of coarse particle nitrate aerosol, Atmos. Environ., 30, 2475-2482, https://doi.org/10.1016/1352-2310(95)00492-0, 1996.

Pöschl, U.: Atmospheric aerosols: Composition, transformation, climate and health effects, Angew. Chem. Int. Ed., 44, 7520-7540, https://doi.org/10.1002/anie.200501122, 2005.

Skamarock, W.C., and coauthors: A Description of the Advanced Research WRF Version 3. NCAR Technical Notes, NCAR/TN-4751STR, doi:10.5065/D68S4MVH, 2008.

Seinfeld, J. H, and Pandis, S. N.: Atmospheric Chemistry and Physics: From air pollution to climate change, John Wiley & Sons, New York, 2006.

Shi, G. L., Tian, Y. Z., Han, S. Q., Zhang, Y. F., Li, X., Feng, Y. C., Wu, J. H., and Zhu, T.: Vertical characteristics of carbonaceous species and their source contributions in a Chinese mega city, Atmos. Environ., 60, 358-365, https://doi.org/10.1016/j.atmosenv.2012.06.069, 2012.

Sun, Y. L., Wang, Z., Fu, P. Q, Jiang, Q., Yang, T., Li, J., and Ge, X. L.: The impact of relative humidity on aerosol composition and evolution processes during wintertime in Beijing, China, Atmos. Environ., 77, 927-934, https://doi.org/10.1016/j.atmosenv.2013.06.019, 2013.

Sun, Y. L., Du, W., Wang, Q. Q., Zhang, Q., Chen, C., Chen, Y., Chen, Z., Fu, P. Q., Wang, Z., Gao, Z., and Worsnop, D. R.: Real-Time Characterization of Aerosol Particle Composition above the Urban Canopy in Beijing: Insights into the

© Author(s) 2019. CC BY 4.0 License.

Interactions between the Atmospheric Boundary Layer and Aerosol Chemistry, Environ. Sci. Technol., 49, 11340-11347, doi: 10.1021/acs.est.5b02373, 2015.

Tao, J., Zhang, Z. S., Tan, H. B, Zhang, L. M., Wu, Y. F., Sun, J. R., Che, H. Z., Cao, J. J., Cheng, P., Chen, L. G., and Zhang, R. J.: Observational evidence of cloud processes contributing to daytime elevated nitrate in an urban atmosphere, Atmos. Environ., 186, 209-215, https://doi.org/10.1016/j.atmosenv.2018.05.040, 2018.

Tian, S. L., Pan, Y. P., and Wang, Y. S.: Size-resolved source apportionment of particulate matter in urban Beijing during haze and non-haze episodes, Atmos. Chem. Phys., 16, 1-19, https://doi.org/10.5194/acp-16-1-2016, 2016.

Wall, S. M., John, W., and Ondo, J. L.: Measurement of aerosol size distributions for nitrate and major ionic species, Atmos. Environ. (1967), 22, 1649-1656, https://doi.org/10.1016/0004-6981(88)90392-7, 1988.

Wang, J., Zhou, M., Liu, B. S., Wu, J. H., Peng, X., Zhang, Y. F., Han, S. Q., Feng, Y. C., and Zhu, T.: Characterization and source apportionment of size-segregated atmospheric particulate matter collected at ground level and from the urban canopy in Tianjin, Environ. Pollut., 219, 982-992, https://doi.org/10.1016/j.envpol.2016.10.069, 2016.

Wang, G. H., Cheng, C. L., Huang, Y., Tao, J., Ren, Y. Q., Wu, F., Meng, J. J., Li, J. J., Cheng, Y. T., Cao, J. J., Liu, S. X., Zhang, T., Zhang, R., and Chen, Y. B.: Evolution of aerosol chemistry in Xi'an, inland China, during the dust storm period of - Part 1: Sources, chemical forms and formation mechanisms of nitrate and sulfate, Atmos. Chem. Phys., 14, 11571–11585, https://doi.org/10.5194/acp-14-11571-2014, 2014.

Wang, Q. Q, Sun, Y. L., Xu, W. Q., Du, W., Zhou, L. B., Tang, G. Q., Chen, C., Cheng, X. L., Zhao, X. J., Ji, D. S., Han, T. T., Wang, Z., Li, J., and Wang, Z. F.: Vertically resolved characteristics of air pollution during two severe winter haze episodes in urban Beijing, China, Atmos. Chem. Phys., 18, 2495-2509, https://doi.org/10.5194/acp-18-2495-2018, 2018.

Wang, X. F., Wang, W. X., Yang, L. X., Gao, X. M., Nie, W., Yu, Y. C., Xu, P. J., Zhou, Y., and Wang, Z.: The secondary formation of inorganic aerosols in the droplet mode through heterogeneous aqueous reactions under haze conditions, Atmos. Environ., 63, 68-76, http://dx.doi.org/10.1016/j.atmosenv.2012.09.029, 2012.

Wu, M., Wu, D., Fan, Q., Wang, B. M., Li, H. W., and Fan, S. J.: Observational studies of the meteorological characteristics associated with poor air quality over the Pearl River Delta in China, Atmos. Chem. Phys., 13(21), 10755-10766, doi:10.5194/acp-13-10755-2013, 2013.

Wu, P. M., and Okada, K.: Nature of coarse nitrate particles in the atmosphere—a single particle approach, Atmos. Environ., 28, 2053-2060, https://doi.org/10.1016/1352-2310(94)90473-1, 1994.

Yao, X. H., Lau, A. P. S., Fang, M., Chan, C. K., and Hu, M.: Size distributions and formation of ionic species in atmospheric particulate pollutants in Beijing, China: 1-inorganic ions, Atmos. Environ., 37, 2991-3000, http://dx.doi.org/10.1016/S1352-2310(03)00255-3, 2003.

Yun, H., Wang, W. H., Wang, T., Xia, M., Yu, C., Wang, Z., Poon, S. C. N., Yue, D. L., and Zhou, Y.: Nitrate formation from heterogeneous uptake of dinitrogen pentoxide during a severe winter haze in southern China, Atmos. Chem. Phys., 18(23), 17515-17527, https://doi.org/10.5194/acp-18-17515-2018, 2018.

Zauli Sajani, S., Marchesi, S., Trentini, A., Bacco, D., Zigola, C., Rovelli, S., Ricciardelli, I., Maccone, C., Lauriola, P.,

© Author(s) 2019. CC BY 4.0 License.

Cavallo, D. M., Poluzzi, V., Cattaneo, A., and Harrison, R. M.: Vertical variation of $PM_{2.5}$ mass and chemical composition, particle size distribution, NO_2, and BTEX at a high rise building, Environ. Pollut., 235, 339-349, https://doi.org/10.1016/j.envpol.2017.12.090, 2018.

Zhang, R. Y., Wang, G. H., Guo, S., Zamora, M. L., Ying, Q., Lin, Y., Wang, W. G., Hu, M., and Wang, Y.: Formation of Urban Fine Particulate Matter, Chem. Rev., 115(10), 3803-3855, doi: 10.1021/acs.chemrev.5b00067, 2015.

Zhang, Y. F., Xu, H., Tian, Y. Z., Shi, G. L., Zeng, F., Wu, J. H., Zhang, X. Y., Li, X., Zhu, T., and Feng, Y. C.: The study on vertical variability of PM_{10} and the possible sources on a 220 m tower, in Tianjin, China, Atmos. Environ., 45, 6133-6140, http://dx.doi.org/10.1016/j.atmosenv.2011.08.040, 2011.

Zhang, Y. H., Hu, M., Zhong, L. J., Wiedensohler, A., Liu, S., Andreae, M. O., Wang, W., and Fan, S. J.: Regional integrated experiments on air quality over Pearl River Delta 2004 (PRIDE-PRD2004): Overview, Atmos. Environ., 42, 6157-6173, https://doi.org/10.1016/j.atmosenv.2008.03.025, 2008.

Zhao, Y. L., and Gao, Y.: Mass size distributions of water-soluble inorganic and organic ions in size-segregated aerosols over metropolitan Newark in the US east coast, Atmos. Environ., 42, 4063-4078, https://doi.org/10.1016/j.atmosenv.2008.01.032, 2008.

Zheng, G. J., Duan, F. K., Su, H., Ma, Y. L., Cheng, Y., Zheng, B., Zhang, Q., Huang, T., Kimoto, T., Chang, D., Pöschl, U., Cheng, Y. F., and He, K. B.: Exploring the severe winter haze in Beijing: The impact of synoptic weather, regional transport and heterogeneous reactions, Atmos. Chem. Phys., 15, 2969–2983, https://doi.org/10.5194/acp-15-2969-2015, 2015.

Zhou, S. Z., Wang, T., Wang, Z., Li, W. J., Xu, Z., Wang, X. F., Yuan, C., Poon, C. N., Louie, Peter K.K., Luk, Connie W.Y., and Wang, W. X: Photochemical evolution of organic aerosols observed in urban plumes from Hong Kong and the Pearl River Delta of China, Atmos. Environ., 88, 219–229, http://dx.doi.org/10.1016/j.atmosenv.2014.01.032, 2014.

Zhuang, H., Chan, C. K., Fang, M., and Wexler, A. S.: Size distributions of particulate sulfate, nitrate, and ammonium at a coastal site in Hong Kong, Atmos. Environ. 33, 843-853, http://dx.doi.org/10.1016/S1352-2310(98)00305-7, 1999a.

Zhuang, H., Chan, C. K., Fang, M., and Wexler, A. S.: Formation of nitrate and non-sea-salt sulfate on coarse particles, Atmos. Environ., 33, 4223-4233, http://dx.doi.org/10.1016/S1352-2310(99)00186-7, 1999b.

© Author(s) 2019. CC BY 4.0 License.

List of Figure Captions

Figure 1. Map showing the PRD region and Canton Tower sampling sites in Guangdong Province. The red contour indicates the spatial distribution of urban areas from global Land Cover data 2015 (www.esa-landcover-cci.org).

Figure 2. $PM_{2.5}$ mass and chemical components concentrations at ground level (GND), 118 m and 488 m during the (a) autumn and (b) winter sampling periods. The dates at x-axis were the sampling days. The stacked bar diagrams at each day represented chemical components at ground level (left), 118 m (middle) and 488 m (right). The green lines represent the daily averaged $PM_{2.5}$ mass concentration. E1 and E2 represent two haze episodes with daily average $PM_{2.5}$ concentrations on the ground site higher than 75 μg m^{-3}.

Figure 3. Representative and average vertical profiles of sulfate, ammonium, nitrate, OC, and EC mass concentration at ground level, 118 m and 488 m during (a) autumn; (b) winter. Four layers of $PM_{2.5}$ mass concentrations were shown here with the data measured by Guangzhou Environmental Monitoring Centre.

Figure 4. Relative importance of the main chemical components in (a) fine mode and (b) coarse mode particles at three different levels of Canton Tower.

Figure 5. Mass concentration size distributions of the main chemical components measured at ground level, 118 m and 488 m in autumn. The dotted lines represent nonlinear fitting of the measured average size distribution.

Figure 6. Mass concentration size distributions of the main chemical components measured at ground level, 118 m and 488 m in winter. The dotted lines represent nonlinear fitting of the measured average size distribution.

Figure 7. Vertical profiles of relative humidity and tempreture modeled by WRF for (a) E1 during autumn and (b) E2 during winter field studies as marked in the Fig. 2.

Figure 8. The distribution of vertical wind (color scale, red: upward; blue: downward) and cloud fraction (black contour line) simulated by the WRF model during (a) autumn and (b) winter episodes.

Figure 9. A schematic graph for illustrating typical haze formation mechanisms in the PRD region in autumn and winter.

Atmos. Chem. Phys. Discuss., https://doi.org/10.5194/acp-2019-155
Manuscript under review for journal Atmos. Chem. Phys.
Discussion started: 4 March 2019
© Author(s) 2019. CC BY 4.0 License.

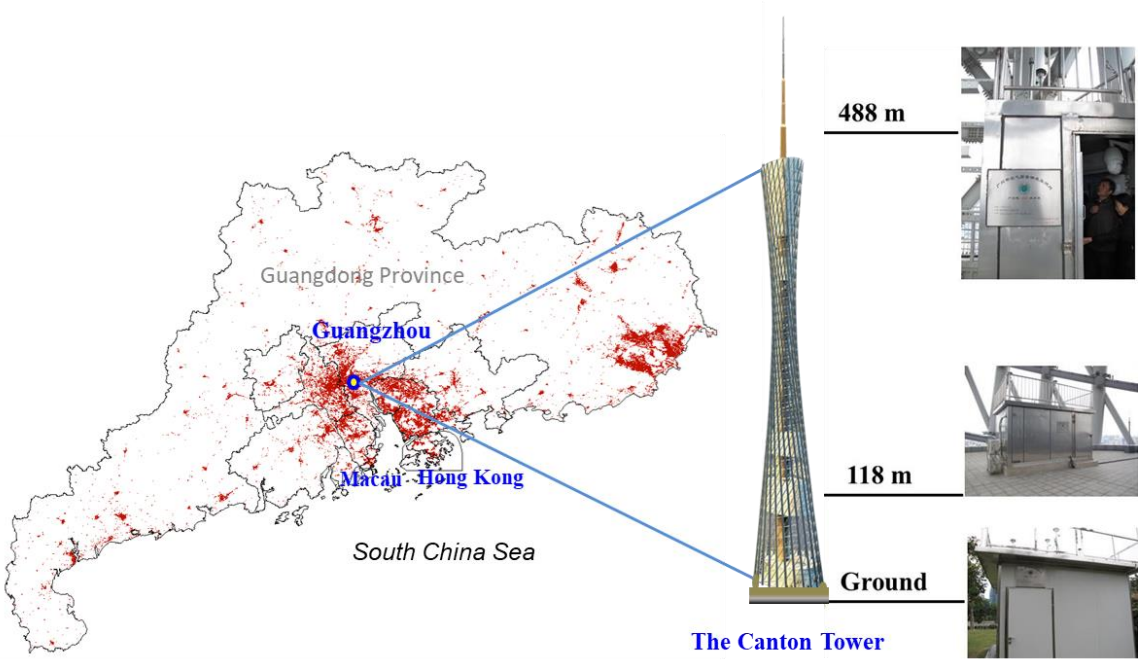

Figure 1. Map showing the PRD region and Canton Tower sampling sites in Guangdong Province. The red contour indicates the spatial distribution of urban areas from global Land Cover data 2015 (www.esa-landcover-cci.org).

Atmos. Chem. Phys. Discuss., https://doi.org/10.5194/acp-2019-155
Manuscript under review for journal Atmos. Chem. Phys.
Discussion started: 4 March 2019
© Author(s) 2019. CC BY 4.0 License.

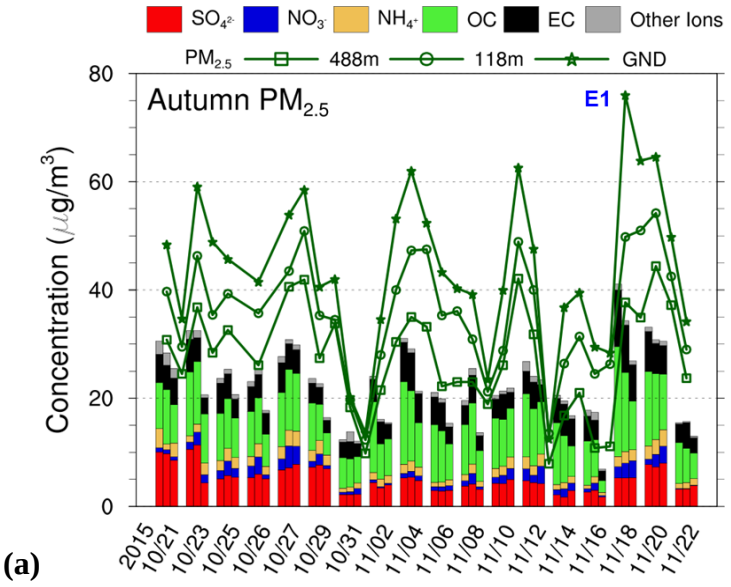

(a)

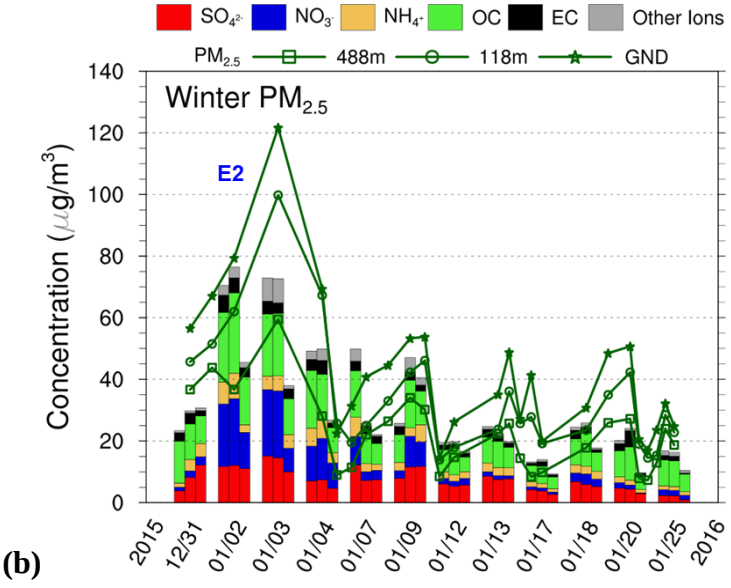

(b)

Figure 2. $PM_{2.5}$ mass and chemical components concentrations at ground level (GND), 118 m and 488 m during the (a) autumn and (b) winter sampling periods. The dates at x-axis were the sampling days. The stacked bar diagrams at each day represented chemical components at ground level (left), 118 m (middle) and 488 m (right). The green lines represent the daily averaged $PM_{2.5}$ mass concentration. E1 and E2 represent two haze episodes with daily average $PM_{2.5}$ concentrations on the ground site higher than 75 μg m^{-3}.

Atmos. Chem. Phys. Discuss., https://doi.org/10.5194/acp-2019-155
Manuscript under review for journal Atmos. Chem. Phys.
Discussion started: 4 March 2019
© Author(s) 2019. CC BY 4.0 License.

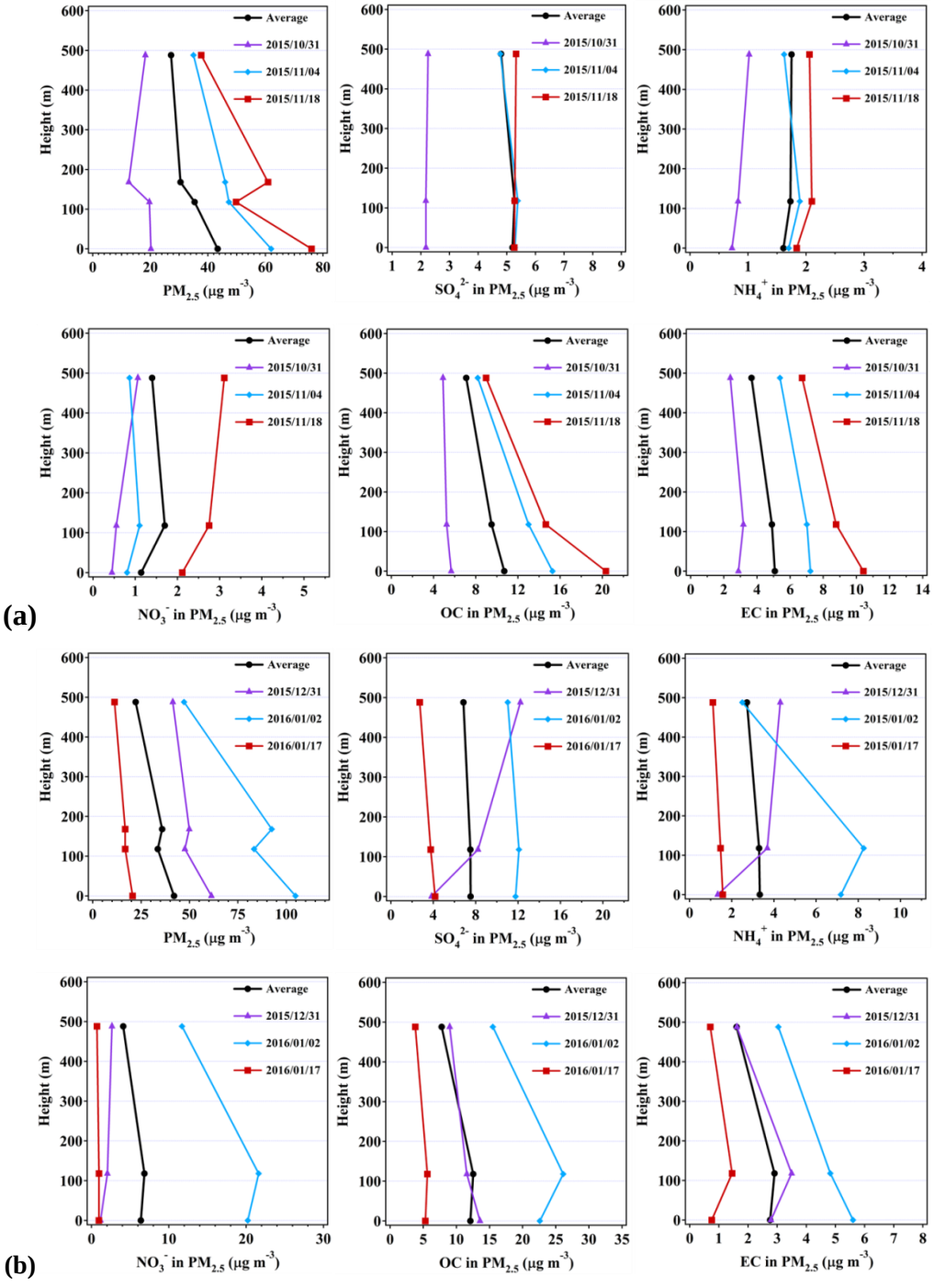

Figure 3. Representative and average vertical profiles of sulfate, ammonium, nitrate, OC, and EC mass concentration at ground level, 118 m and 488 m during (a) autumn; (b) winter. Four layers of $PM_{2.5}$ mass concentrations were shown here with the data measured by Guangzhou Environmental Monitoring Centre.

Atmos. Chem. Phys. Discuss., https://doi.org/10.5194/acp-2019-155
Manuscript under review for journal Atmos. Chem. Phys.
Discussion started: 4 March 2019
© Author(s) 2019. CC BY 4.0 License.

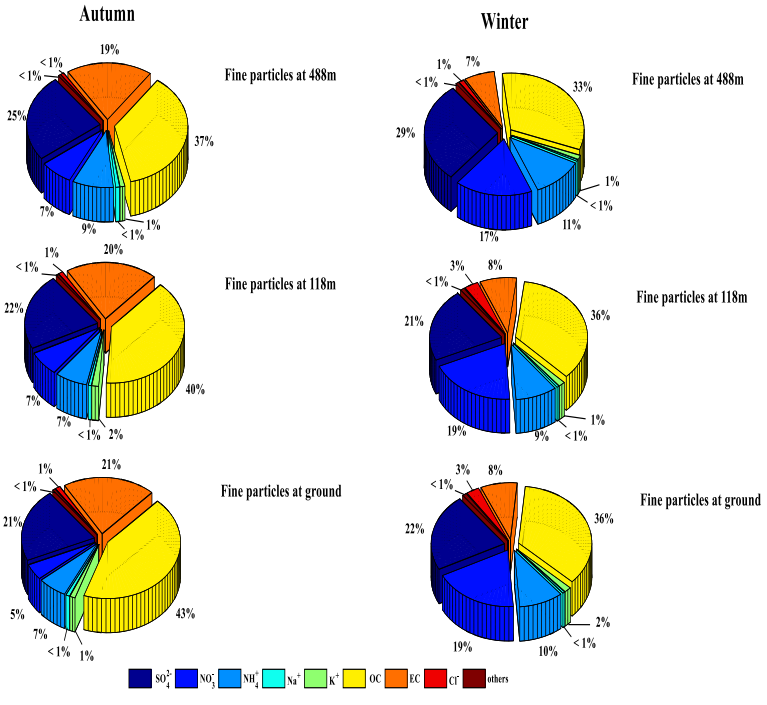

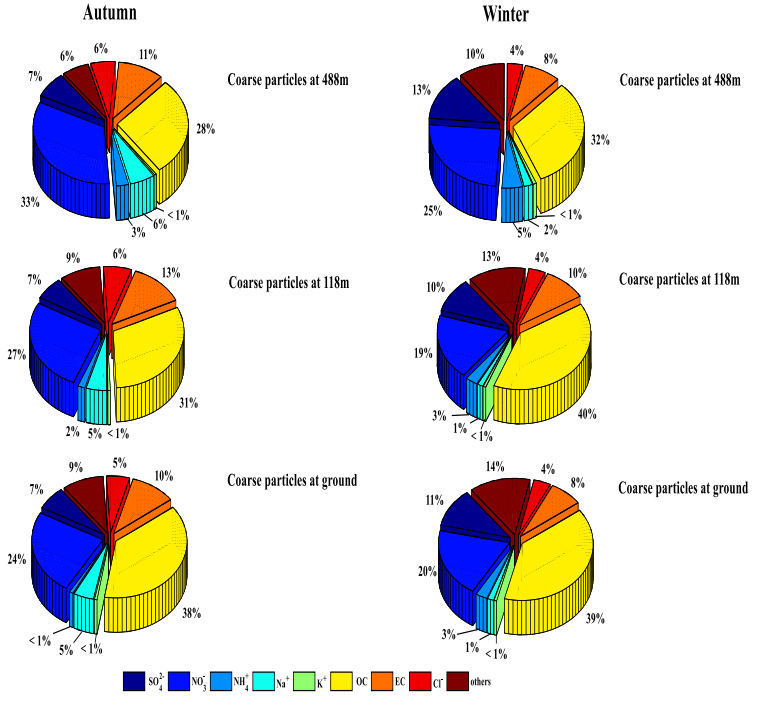

Figure 4. Relative importance of the main chemical components in (a) fine mode and (b) coarse mode particles at three different levels of Canton Tower.

Atmos. Chem. Phys. Discuss., https://doi.org/10.5194/acp-2019-155
Manuscript under review for journal Atmos. Chem. Phys.
Discussion started: 4 March 2019
© Author(s) 2019. CC BY 4.0 License.

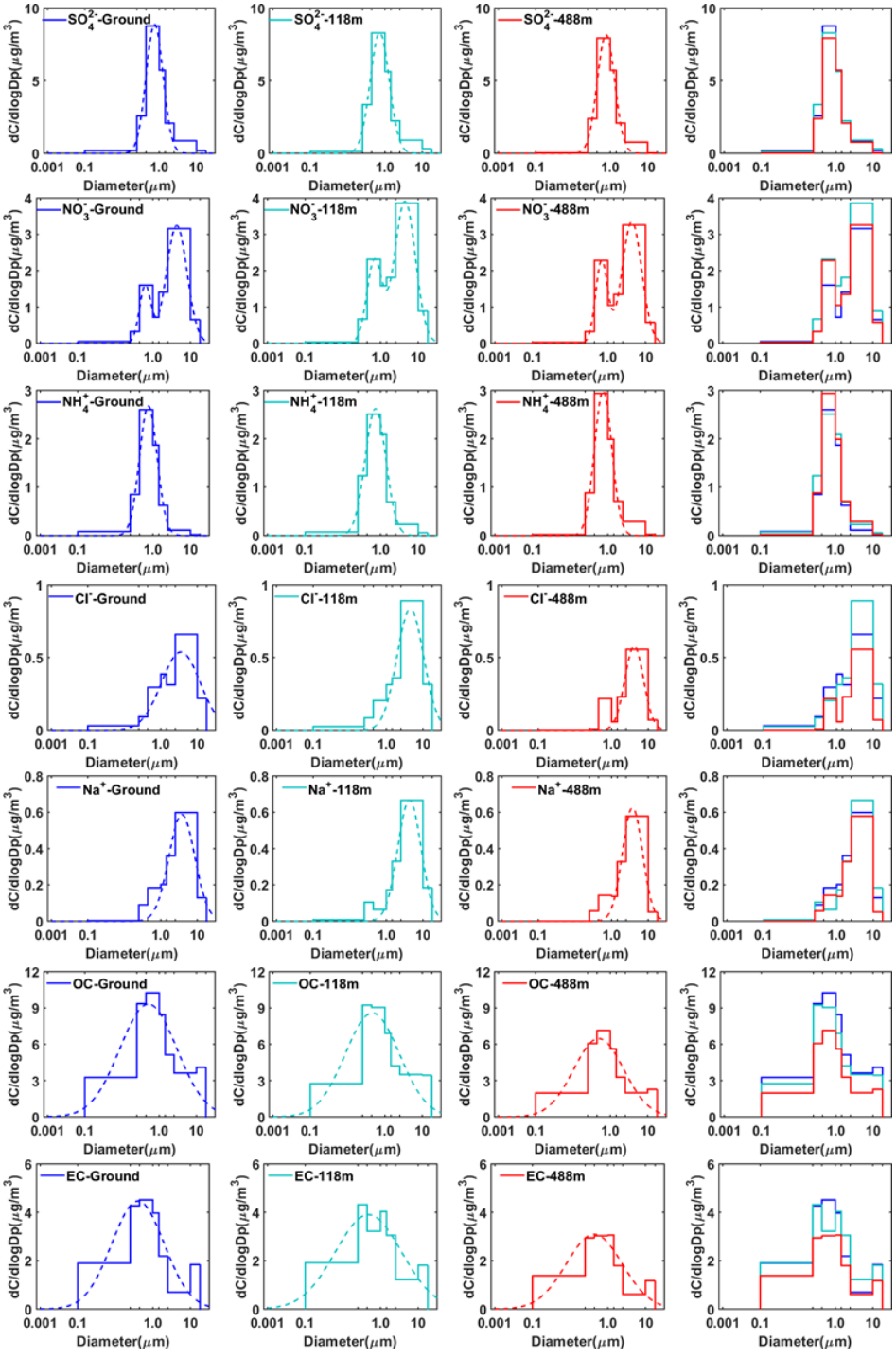

Figure 5. Mass concentration size distributions of the main chemical components measured at ground level, 118 m and 488 m in autumn. The dotted lines represent nonlinear fitting of the measured average size distribution.

Atmos. Chem. Phys. Discuss., https://doi.org/10.5194/acp-2019-155
Manuscript under review for journal Atmos. Chem. Phys.
Discussion started: 4 March 2019
© Author(s) 2019. CC BY 4.0 License.

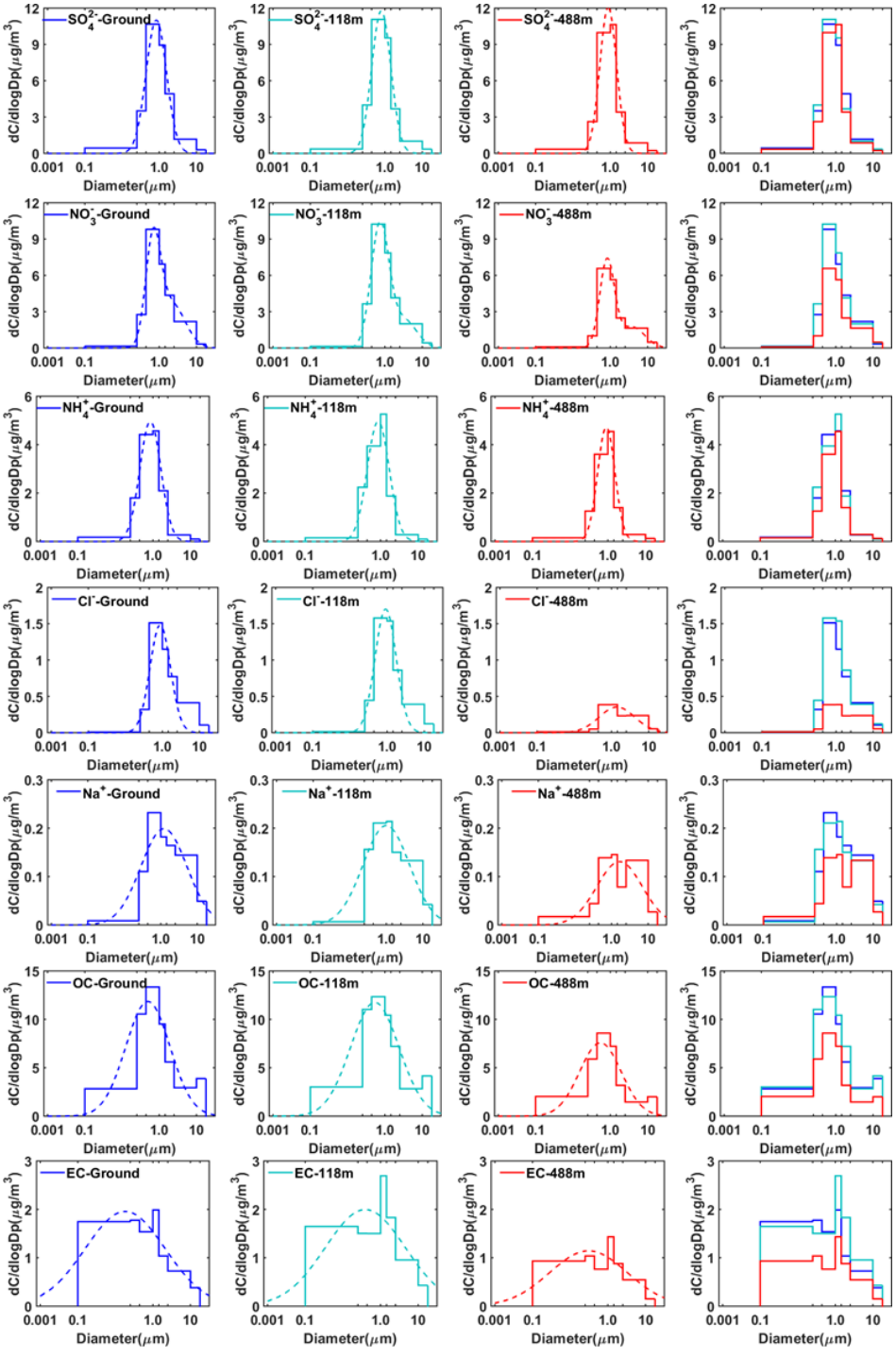

Figure 6. Mass concentration size distributions of the main chemical components measured at ground level, 118 m and 488 m in winter. The dotted lines represent nonlinear fitting of the measured average size distribution.

Atmos. Chem. Phys. Discuss., https://doi.org/10.5194/acp-2019-155
Manuscript under review for journal Atmos. Chem. Phys.
Discussion started: 4 March 2019
© Author(s) 2019. CC BY 4.0 License.

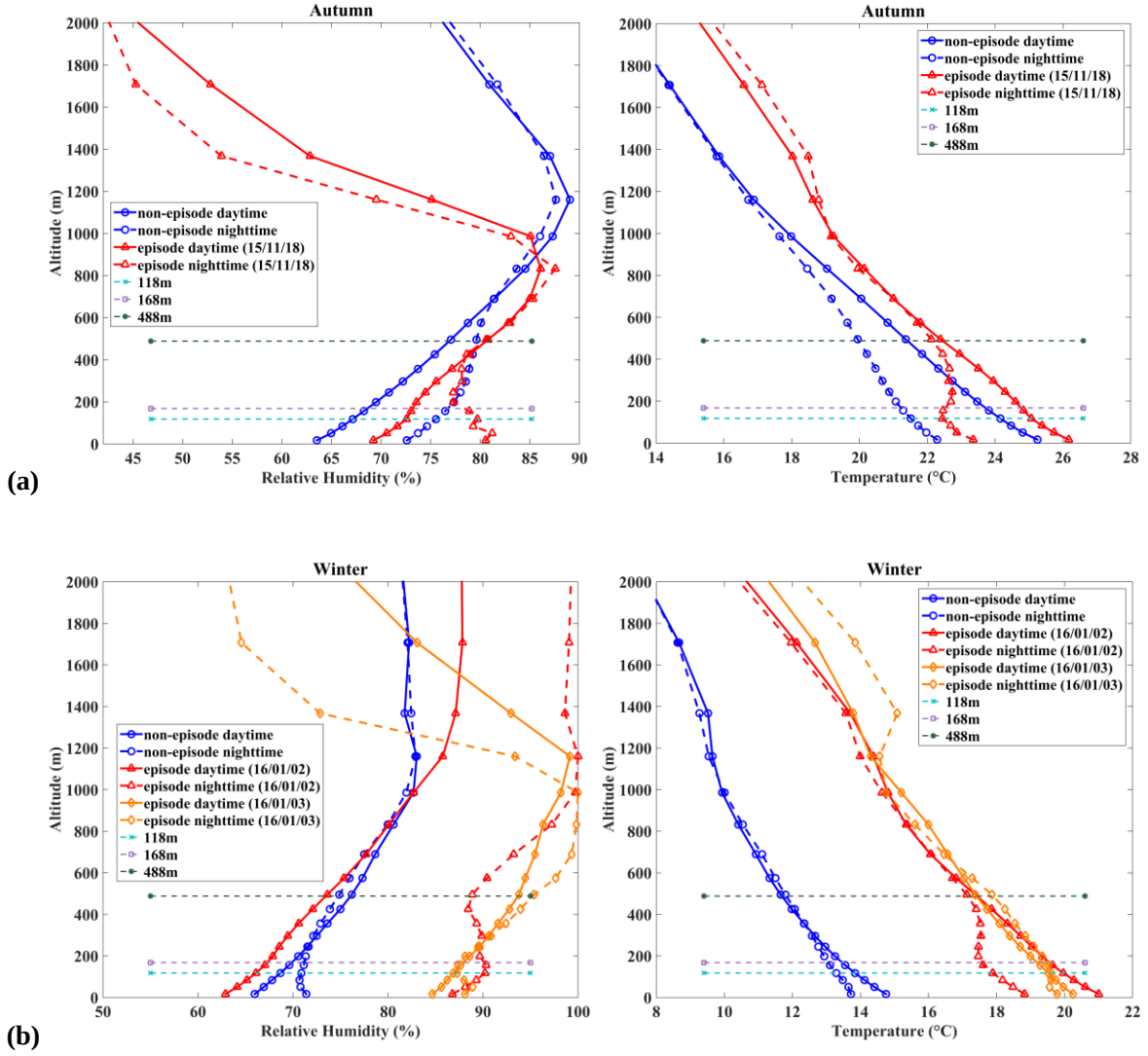

Figure 7. Vertical profiles of relative humidity and tempreture modeled by WRF for (a) E1 during autumn and (b) E2 during winter field studies as marked in the Fig. 2.

Atmos. Chem. Phys. Discuss., https://doi.org/10.5194/acp-2019-155
Manuscript under review for journal Atmos. Chem. Phys.
Discussion started: 4 March 2019
© Author(s) 2019. CC BY 4.0 License.

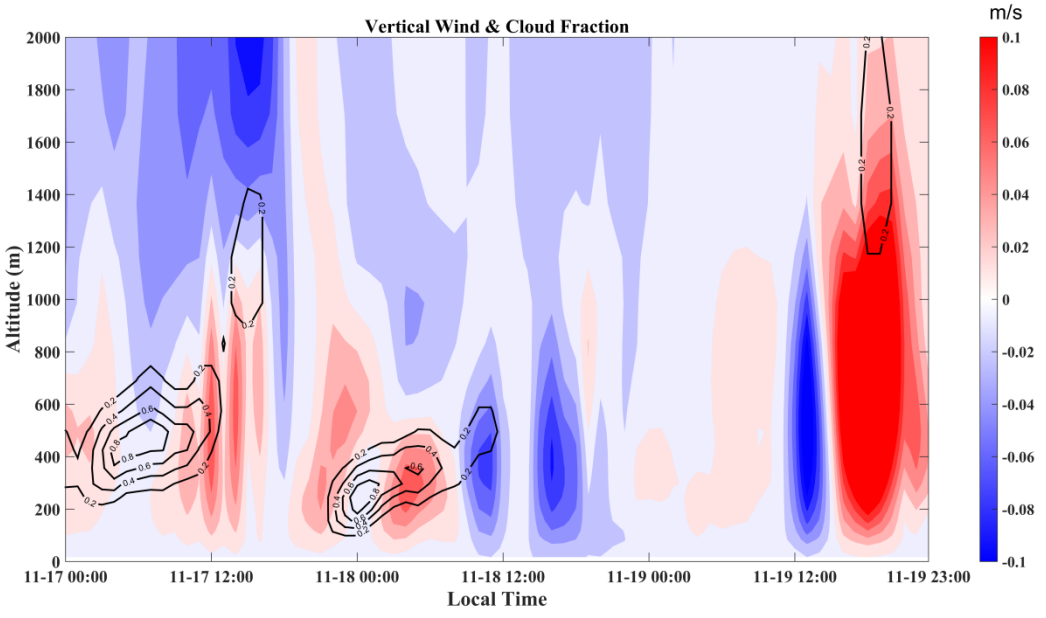

(a)

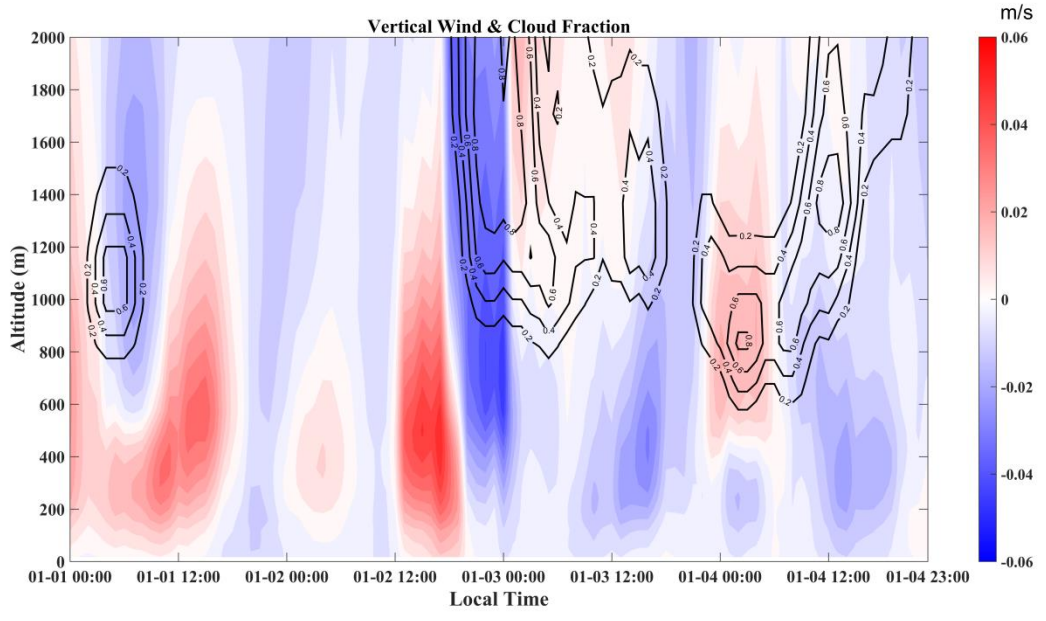

(b)

Figure 8. The distribution of vertical wind (color scale, red: upward; blue: downward) and cloud fraction (black contour line) simulated by the WRF model during (a) autumn and (b) winter episodes.

Atmos. Chem. Phys. Discuss., https://doi.org/10.5194/acp-2019-155
Manuscript under review for journal Atmos. Chem. Phys.
Discussion started: 4 March 2019
© Author(s) 2019. CC BY 4.0 License.

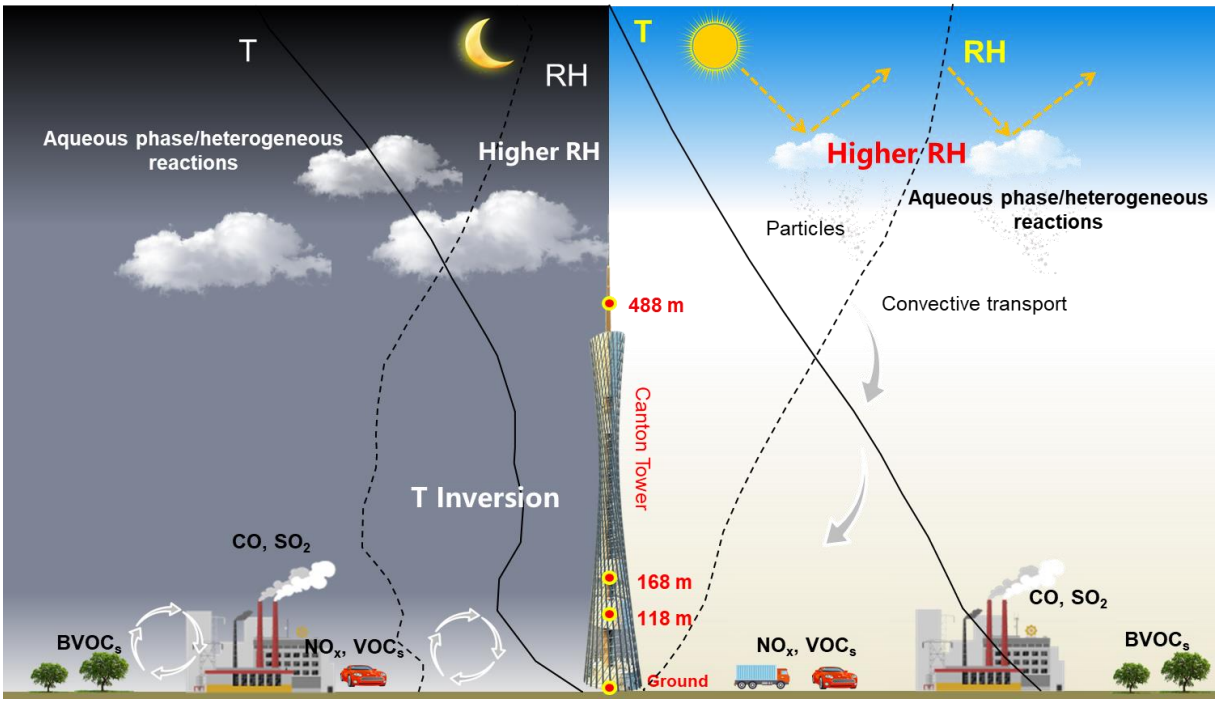

Figure 9. A schematic graph for illustrating typical haze formation mechanisms in the PRD region in autumn and winter.